ACS Catalysis

pubs.acs.org/acscatalysis Research Article

Individual Functionality and Synergistic Effects of Redox Site−Acid Site in Propane Oxidation

Cai-Hao Wen, Lin-Ya Xu, Yao-Dong Hao, Qian Zhou, Yi-Wei Xian, Mao-Di Wang,* Wei Tan,* Lin Dong, Jian Chen,* Meng-Fei Luo, and Qi-Hua Yang

Cite This: *ACS Catal.* 2025, 15, 10746−10757 Read Online

ACCESS | Metrics & More | Article Recommendations | Supporting Information

ABSTRACT: Catalytic combustion represents one of the most efficient technologies for light-alkane volatile organic compound abatement. However, the reaction mechanisms over heterogeneous catalysts remain controversial, which significantly hinders the rational design of highly efficient and stable catalysts. In this work, it is found that the T_{50} (the temperature at which propane conversion reached 50%) of Pt/MoO_3 (220 °C) is much lower than that of Pt/CeO_2 (T_{50} = 320 °C) in propane combustion ($C_3H_8 + O_2 \rightarrow CO_2 + H_2O$), indicating the possibility of synergistic catalysis occurring between Pt and MoO_3 sites. Based on a hybrid catalysis system composed of physically mixed MoO_3 and Pt/CeO_2 (denoted as Pt/CeO_2+MoO_3), the critical roles of the acid site from MoO_3 for propane activation and the Pt site for oxygen-activation have been originally investigated in propane oxidation, even though Pt and MoO_3 sites are spatially separated. The results of the kinetic study, *in situ* diffuse reflectance infrared Fourier transform spectra of propane combustion, and X-ray photoelectron spectra experiments sufficiently evidenced that propane preferentially absorbs on the MoO_3 surface, and the oxygen spillover from Pt sites to the MoO_3 surface further facilitates the oxidation of propane. Density functional theory calculations reveal that Pt sites exhibit stronger O_2 adsorption, while the synergy between five-coordinated and four-coordinated Mo sites enables MoO_3 with an enhanced propane activation capability. That is, MoO_3 offers important extra sites for propane activation, effectively avoiding the competitive adsorption between oxygen and propane on the Pt sites. A large distance between MoO_3 and Pt sites negatively impacts catalytic activity. Additionally, via construction of defective MoO_3 containing more surface acid sites, it is disclosed that stronger surface acidity of MoO_3 significantly promotes the catalytic performance of Pt sites and MoO_3 sites. This work sheds light on the reaction mechanism of light-alkane oxidation over the metal oxide-supported Pt catalyst.

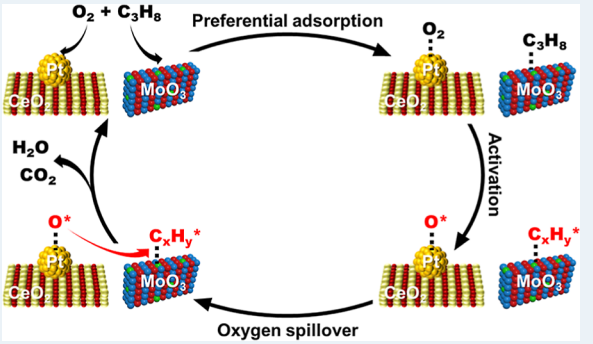

KEYWORDS: *propane activation, synergistic catalysis, MoO_3 defects, surface acid sites, Pt active sites, oxygen spillover*

1. INTRODUCTION

The intensive emission of volatile organic compounds (VOCs), regarded as hazardous atmospheric pollutants, has caused serious environmental issues. Among those VOCs, light alkanes with stable chemical structures are the most difficult to be eliminated.[1−3] Liquified petroleum gas, a mixture of light alkanes (propane and butanes), has been widely employed as the main gasoline substitute for automobiles. During the cold-start process, the catalytic converter cannot effectively oxidize the light alkanes and CO into harmless CO_2 and water.[4−6] Thus, the development of low-light-off alkane oxidation catalysts is a promising approach toward the removal of light alkanes in automotive exhaust.

It is generally recognized that noble metal (Pt, Pd, Ru, etc.)-based catalytic materials are most active for catalytic combustion of light alkanes due to their superior ability for C−H activation; thus, noble metal components are widely present in commercial catalysts for exhaust gas elimination.[7−12] Particularly, it has been reported that Pt catalysts exhibit superior catalytic activity than Pd catalysts for the catalytic oxidation of light alkanes (C_nH_{2n+2}, $n \geq 2$).[13,14] Considering the scarcity, irreplaceability, and high cost of Pt metal, increasing efforts have been paid to increase the activity of the Pt catalyst to save the utilization of Pt metal. However, most of the researchers' attention has been drawn by tuning the nature of Pt active sites, such as morphology, size effect, surface valence state, etc.[15−17] For example, metallic Pt species are considered to effectively activate the C−H bond while the oxidized Pt species enable the subsequent hydrocarbon oxidation.[18] However, the suitable ratio of metallic to oxidized Pt species remains unclear. The support effect has also been

Received: April 13, 2025
Revised: May 23, 2025
Accepted: May 27, 2025

https://doi.org/10.1021/acscatal.5c02534
ACS Catal. 2025, 15, 10746−10757

studied in Pt catalysts for light alkane combustion.[19,20] Most of the viewpoints in previous works consistently agree that Pt catalysts supported on acidic materials are more conducive to alkane combustion because acidic materials benefit Pt species to be stabilized in the metallic state.[21−24] Although the important role of acid sites on alkanes activation has drawn extensive attention in the fields of alkane isomerization or upcycling of waste plastic,[25,26] such promotion of acidic support on light alkane activation during catalytic combustion has been seriously underestimated so far, compared to the numerous studies on Pt sites.

Acquiring accurate knowledge about the active sites of a catalyst and the reaction mechanism of light alkane oxidation on heterogeneous catalyst surfaces is useful for designing efficient catalysts but is exceedingly challenging. Unlike methane combustion reaction commonly recognized to follow the Mars-van Krevelen mechanism on a noble metal-based catalyst,[27] the oxidation of propane, a representative light-alkane volatile organic compound, is mostly discussed to be proceeded by the Langmuir−Hinshelwood mechanism (L−H).[28,29] However, the competitive adsorption between gaseous oxygen and propane on Pt-active sites results in the decrease of catalytic activity when the oxygen partial pressure increased. Generation of interface active sites between Pt and transition metal oxide support (such as Pt−O−W and Pt−O−Mo) may benefit gaseous oxygen activation and then increase the total reaction rate.[30,31] Besides, Xu et al. clarified that solid acid sites ($AlSO_x$) play critical roles in propane activation, and noble metal Pt sites mainly activate the gaseous oxygen, thus avoiding the competitive adsorption and accelerating propane oxidation reaction.[32] Moreover, it can be seen that the active sites with strong C−H activation ability are not limited to noble metal sites, and acidic sites may be more active toward C−H or C−C bonds of light alkanes.[33−37] Achieving effective synergistic catalysis on a catalyst containing multiactive sites not only improves its catalytic activity but also saves the usage of noble metals. However, the understanding of synergistic catalysis on supported Pt catalysts is still barely studied, especially for Pt catalysts supported on acidic transition metal oxides.

Due to the nature of MoO_3 in tuning the electronic structure of supported Pt species, MoO_3 has been taken as a promising support for the construction of efficient Pt catalysts for the combustion of VOCs. In addition, MoO_3 also contains sufficient acidic sites and oxygen vacancies,[38] which not only facilitate the adsorption and activation of VOCs but also promote the rapid mobility of oxygen species. In this work, to further differentiate the roles of acid sites and Pt sites in the propane oxidation reaction, Pt/MoO_3, Pt/CeO_2, and a hybrid catalysis system composed of MoO_3 and Pt/CeO_2 were prepared and used as model catalysts. Our catalyst evaluations and characterizations reveal that the surface acid sites from MoO_3 play critical roles in propane adsorption/activation, and oxygen spillover from Pt active sites to the MoO_3 surface promotes propane oxidation. Such a synergistic catalysis mechanism proposed in this work is different from the traditional viewpoint that propane activation mainly occurs on noble metal active sites and provides deep insights into the development of efficient Pt catalysts for propane oxidation.

2. EXPERIMENTAL SECTION

2.1. Catalyst Preparation. CeO_2, MoO_3, and ZrO_2 supports were synthesized by calcination of $Ce(NO_3)_3{\cdot}6H_2O$, $(NH_4)_6Mo_7O_{24}{\cdot}4H_2O$, and $ZrOCO_3$, respectively, at 500 °C with a ramping rate of 10 °C·min^{-1} in static air for 4 h.

A typical impregnation method was adopted to deposit 1 wt % Pt on CeO_2 and MoO_3 support for the preparation of Pt/CeO_2 and Pt/MoO_3 catalysts. Specifically, 1 g support (CeO_2 or MoO_3) was added to the aqueous solution of $Pt(NO_3)_2$ (5 mL, 0.002 mg·L^{-1}), and the mixture was stirred at room temperature for 3 h and then evaporated at 90 °C. Afterward, the solid was dried in an oven at 100 °C for 12 h, followed by calcination in static air at 500 °C for 4 h with a ramping rate of 10 °C·min^{-1}.

Pt/CeO_2+MoO_3 represents the physical mixture of Pt/CeO_2 and MoO_3, and "+" stands for physical mixture. Typically, the same weights (0.05 g) of Pt/CeO_2 and MoO_3 were mixed and grounded for 15 min to achieve a uniform mixture, which was then pressed and sieved (60−80 mesh). In contrast, (Pt/CeO_2) + (MoO_3) represents the mixed catalysis systems composed of individually pressed and sieved (60−80 mesh) particles of Pt/CeO_2 and MoO_3.

2.2. Characterizations. The crystallinity of the catalyst was investigated by using powder X-ray diffraction (XRD). The samples were analyzed using a Bruker D8 diffractometer with Cu Kα radiation operating at 40 kV and 40 mA. The scan speed was 12°·min^{-1} over the 2θ range of 10−90°. The Brunauer−Emmet−Teller (BET) surface area of the catalyst was determined by means of nitrogen adsorption at 77 K using a BK 200 C apparatus. Raman spectra were recorded by a confocal microprobe Raman system (Renishaw in Via Reflex) with an excitation laser of 325 nm (laser power = 10 mW, dwell time = 60 s, number of scans = 100, and resolution = 1 cm^{-1}). High-resolution transition electron microscopy (HRTEM) images were obtained on a JEOL-2100F instrument operated at 200 kV. The NH_3-temperature-programmed desorption (NH_3-TPD) experiment was performed on the self-made tubular quartz reactor equipped with a thermal conductivity detector (TCD). Prior to the test, the catalyst (50 mg, 60−80 mesh) was put in the reactor and pretreated in N_2 flow (20 mL·min^{-1}) under 300 °C for 0.5 h and cooled down to 40 °C. Then, high-purity NH_3 gas was flowed into the reactor (30 mL·min^{-1}) for 10 min, and N_2 flow (20 mL·min^{-1}) was purged for 0.5 h to clean the gaseous or physically adsorbed NH_3 on catalysts. Subsequently, the catalyst was heated from 40 to 700 °C in high-purity N_2 flow (20 mL·min^{-1}) to desorb the chemical adsorption NH_3, and outlet gas from the reactor was dehydrated by KOH and then introduced into the TCD detector to record the NH_3 signal. The relative NH_3 desorption amount was calculated by the area of the NH_3-desorption peak. X-ray photoelectron spectra (XPS) were recorded using an ESCALAB 250Xi instrument with Al Kα source ($h\nu$ = 1484.6 eV), and the binding energy was calibrated by C 1s XPS centered at 284.8 eV. The XPS spectra were deconvoluted using XPSPEAK41 software. For the propane temperature-programmed surface reaction (C_3H_8-TPSR), 100 mg of catalyst was heated from 25 to 500 °C with a ramping rate of 10 °C·min^{-1} in a mixture flow of 30 mL·min^{-1} (0.2 vol % C_3H_8/N_2 balance or 0.2 vol % C_3H_8 + 2 vol % O_2/N_2 balance). The components in outlet gas were detected by a mass spectrometer (Hiden HPR-20 R&D), and MS signals at m/z = 16, 29, 30, and 44 were collected for detecting CH_4, C_3H_8, C_2H_6, and CO_2, respectively. For the O_2-temperature-programmed oxidation (O_2-TPO) experiment, 200 mg of Pt/CeO_2, 400 mg of MoO_3-R(-R meant prereduction by H_2 at 200 °C), and 200 mg of Pt/CeO_2 +

https://doi.org/10.1021/acscatal.5c02534
ACS Catal. 2025, 15, 10746−10757

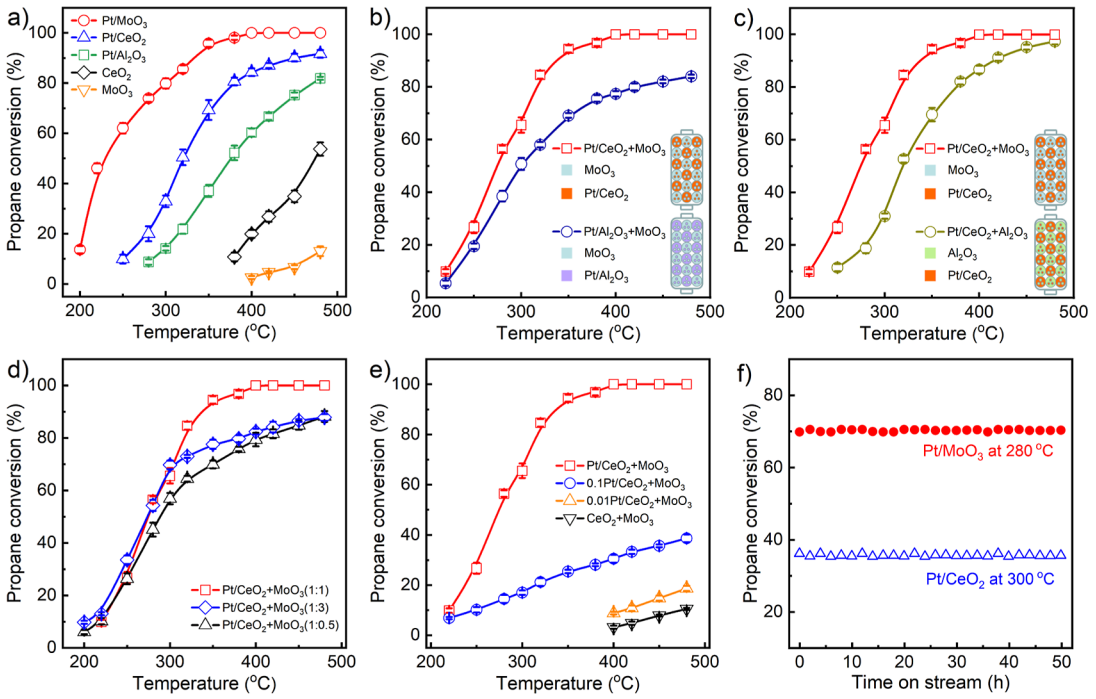

Figure 1. (a) Light-off curves of propane oxidation over catalysts. (b,c) Propane oxidation over a physically mixed catalyst of Pt/CeO_2+MoO_3, $Pt/Al_2O_3+MoO_3$, and $Pt/CeO_2+Al_2O_3$. (d) The effect of mass ratio (provided in bracket) of Pt/CeO_2 to MoO_3 on propane oxidation. (e) The effect of Pt content in Pt/CeO_2 (0.1 and 0.01 means Pt loading (wt %),Pt catalysts with 1 wt % Pt is not marked) on propane oxidation. (f) Stability test of Pt/MoO_3 and Pt/CeO_2.

400 mg of MoO_3-R catalysts were heated from 25 to 550 °C with a ramping rate of 10 °C·min^{-1} in a mixture flow of 30 mL·min^{-1} (0.4 vol % O_2/N_2 balance). The components in outlet gas were detected by a mass spectrometer (Hiden HPR-20 R&D), and MS signal at m/z = 32 was collected for detecting O_2. Thermogravimetry analysis (TGA) was carried out on a NETZSCH STA 449F3 analyzer to test decomposition temperature of activated carbon (C) or physically mixed with the Pt catalyst, with a ramp rate of 10 °C min^{-1}, from 30 to 800 °C under air flow. Electron paramagnetic resonance (EPR) test was conducted on a Bruker EPR EMXplus under 9.8 GHZ. *In situ* diffuse reflectance infrared Fourier transform spectra (DRIFTS) experiment of propane oxidation was carried out on a Thermal-Fischer Nicolet iS50 FT-IR spectrometer equipped with a MCT detector and a PIKE DRIFT accessory. Prior to the test, the catalyst was placed in a PIKE DRIFT accessory and heated in a N_2 atmosphere at 250 °C for 30 min to remove impurities on the catalyst surface before the background spectra were recorded. Afterward, a mixture flow (0.2 vol % C_3H_8 + 2 vol % O_2/N_2 balance, 30 mL·min^{-1}) was introduced into the DRIFTS cell for 60 min at 250 °C, followed by a N_2 flow (30 mL·min^{-1}) for 60 min, and the spectra were recorded, with the background spectra automatically subtracted.

2.3. Catalytic Performance Evaluation. The catalytic performance of the prepared catalysts in the propane combustion reaction was conducted in a quartz tube fixed-bed reactor. In particular, the as-prepared catalyst (60−80 mesh) was placed in a quartz tube with an inner diameter of 6 mm and secured with quartz wool. The reaction temperature was controlled by temperature-programmed equipment. For propane combustion reaction, the reaction mixture gas (66.66 mL·min^{-1}) was composed of 0.2 vol % C_3H_8 and 2 vol % O_2 using N_2 as balance. The weight hourly space velocity based on the mass of Pt was 8,000,000 mL·g_{Pt}^{-1}·h^{-1}). To monitor propane conversion, the inlet and outlet gas of the fixed bed was analyzed by Shimadzu GC-2014 gas chromatography equipped with a flame ionization detector and a HPGS-GASPRO capillary column. Propane conversion was calculated by the following formula

$$\text{Conversion} = ([C_3H_8]_{in} - [C_3H_8]_{out})/[C_3H_8]_{in} \times 100\% \quad (1)$$

where $[C_3H_8]_{in}$ and $[C_3H_8]_{out}$ were the concentrations of propane in the inlet and outlet gas, respectively.

2.4. Kinetic Experiment. Kinetic measurements of propane combustion were conducted under a low propane conversion (< 15%) to exclude the mass transfer and heat transfer effect. The Weisz-Prater formula (CWP) can be applied to exclude the internal diffusion effects, and the Mears criterion (CM) is adopted to exclude both the external diffusion and heat transfer effects. When measuring the reaction orders, the partial pressures of C_3H_8 and O_2 in the propane combustion reaction were controlled at 0.202−0.808 kPa and 1.515−9.09 kPa (Tables S3−S5), respectively. The apparent activation energy (E_a) of the catalyst was calculated based on the reaction rates at different reaction temperatures according to the Arrhenius equation.

2.5. Computational Details. The computational modeling was carried out using density functional theory (DFT) with the Perdew−Burke−Ernzerhof (PBE) functional as implemented in the CP2K package.[39] The spin-polarized wave functions were expanded with a double-ζ atom-centered Gaussian-type basis to describe the wave functions but used an auxiliary planewave basis to describe the density with a 500 Ry energy cutoff.[40] The rest were core electrons, represented by Goedecker−Teter−Hutter (GTH) pseudopotentials. The dispersion correction was applied in all the calculations with

https://doi.org/10.1021/acscatal.5c02534
ACS Catal. 2025, 15, 10746−10757

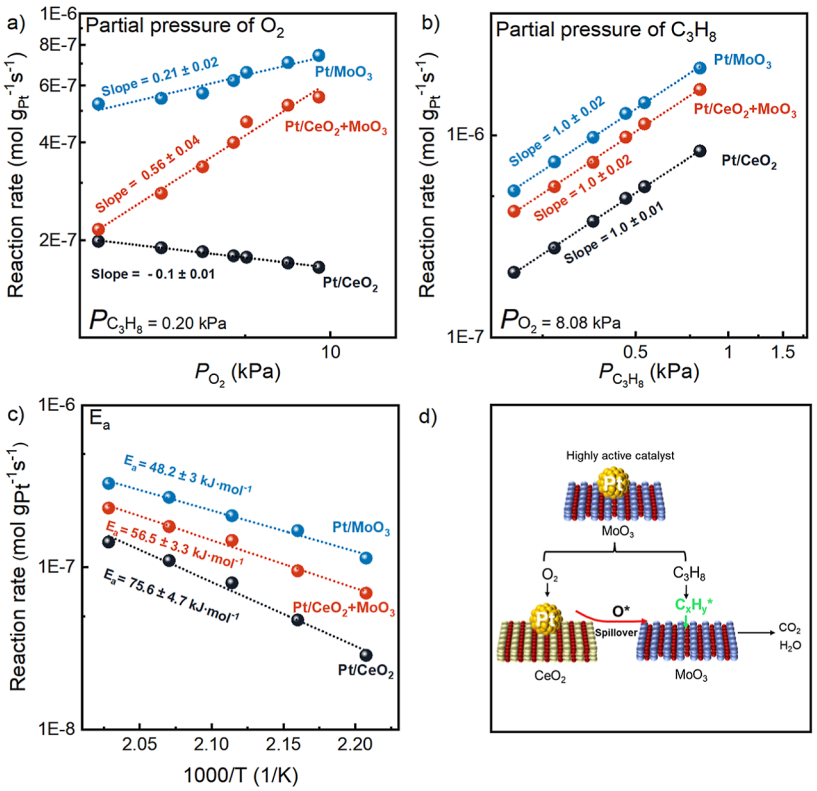

Figure 2. (a,b) Dependence of reaction rate on the partial pressure of O_2 and propane. (c) Arrhenius plots of Pt/MoO_3, Pt/CeO_2, and Pt/CeO_2+MoO_3 catalysts. (d) The proposed reaction mechanism for propane oxidation.

the Grimme-D3 method.[41] The geometry was optimized by the Broyden–Fletcher–Goldfarb–Shanno (BFGS) minimizer with a maximum force of 4.5×10^{-5} Hartrees/Bohr and a root-mean-square force of 3×10^{-4} Hartrees/Bohr. The target accuracy for electron density convergence was 1×10^{-5}. The strongly correlated Ce 4*f* orbitals and Mo 4*d* were treated with the GGA + *U* correction with U_{eff} = 4 and 6 eV.[42,43] The all models were used with a vacuum of 20 Å in the *z* direction of the cell to avoid the interaction with the next periodic layer. The adsorption energy is calculated as $E_{ads} = E_{adsorbate/slab} - E_{slab} - E_{adsorbate}$ (2), where $E_{adsorbate/slab}$ and E_{slab} are the total energies of the slab with the adsorbate and the clean surface, respectively, and $E_{adsorbate}$ is the energy of the adsorbate in the gas phase. The reaction energy was calculated by $\Delta E = E_{FS} - E_{slab} - E_{adsorbate}$ (3), where E_{FS} is the energies of the corresponding final state.

3. RESULT AND DISCUSSION

3.1. Propane Oxidation Performance. MoO_3 containing enriched acid sites was prepared as the support for the loading of Pt nanoparticles. For comparison, Pt/CeO_2 and Pt/Al_2O_3, widely used in catalytic oxidation, were also prepared as benchmarked catalysts. Pt nanoparticles supported on MoO_3, CeO_2, and Al_2O_3 were prepared by a wetness impregnation method and used as model catalysts. XRD patterns and Raman spectra for MoO_3 and CeO_2 as well as the supported Pt catalysts are shown in Figure S1. HRTEM images for Pt/MoO_3 and Pt/CeO_2 are shown in Figure S2. According to the results of XRD, Raman spectra, and HRTEM, smaller Pt particles with average diameters of 2.4 and 1.4 nm were formed on MoO_3 and CeO_2 supports, respectively.

Propane oxidation activities on MoO_3, CeO_2, Pt/MoO_3, Pt/CeO_2, and Pt/Al_2O_3 were evaluated (Figure 1a). Without Pt particles, both CeO_2 and MoO_3 show inferior activity in propane oxidation. CeO_2 exhibits a slightly higher activity than MoO_3, primarily due to its superior redox behavior. Previously, Dong et al. proposed that the overlap of energy levels in the Ce 4*f*–5*d* orbitals, as depicted in the Cotton atomic orbital energy level diagram, enabled the facile conversion between Ce^{3+} and Ce^{4+}, accompanied by the gain/loss of electrons and release/storage of oxygen.[10,44−46] However, in clear contrast, Pt/MoO_3 shows much higher propane oxidation activity than Pt/CeO_2 and Pt/Al_2O_3. Since CeO_2 shows a much better redox performance than MoO_3, the superior propane oxidation activity on Pt/MoO_3 should be more related to the unique states of Pt species or the excellent ability of MoO_3 in propane adsorption and activation.

To further distinguish the role of Pt and MoO_3 sites in the propane oxidation reaction, they are spatially separated by physically mixing catalysts to catalyze propane oxidation. For instance, Pt/CeO_2 physically mixed with equal mass of MoO_3 was denoted as $Pt/CeO_2 + MoO_3$ (+ symbol represents physical mixing). $Pt/CeO_2 + MoO_3$ shows a BET surface area of 31.7 $m^2 \cdot g^{-1}$, which closely matches the arithmetic mean of the two individual components at an equal mass ratio (Table S1). This result suggests that no significant alteration in the pore structure occurred during the physical mixing process of Pt/CeO_2 and MoO_3. It is found that $Pt/CeO_2 + MoO_3$ shows superior catalytic activity than the individual Pt/CeO_2 or MoO_3. Similar results are also observed in the $Pt/Al_2O_3 + MoO_3$ catalyst. However, the $Pt/CeO_2 + Al_2O_3$ catalyst exhibits a comparable activity to the individual Pt/CeO_2 (Figure 1b,c). The above results suggest that the presence of

https://doi.org/10.1021/acscatal.5c02534
ACS Catal. 2025, 15, 10746−10757

Table 1. Kinetic Parameters of Propane Oxidation over Pt/MoO_3, Pt/CeO_2, and $Pt/CeO_2 + MoO_3$ Catalysts[a]

		$r = k_{app}[C_3H_8]^a[O_2]^b$			
catalyst	specific mass reaction rate[a]/mmol g_{cat}^{-1}·h^{-1}	$k_{app}/\times 10^{-7}$	a	b	E_a/kJ mol^{-1}
Pt/CeO_2	0.71	0.7	1.0 ± 0.01	−0.10 ± 0.01	144.7 ± 8.4
Pt/MoO_3	2.65	2.3	1.0 ± 0.02	0.21 ± 0.02	91.9 ± 9.1
$Pt/CeO_2 + MoO_3$	2.05	0.9	1.0 ± 0.02	0.56 ± 0.04	111.4 ± 6.0

[a]Specific mass reaction rate was measured at 250 °C.

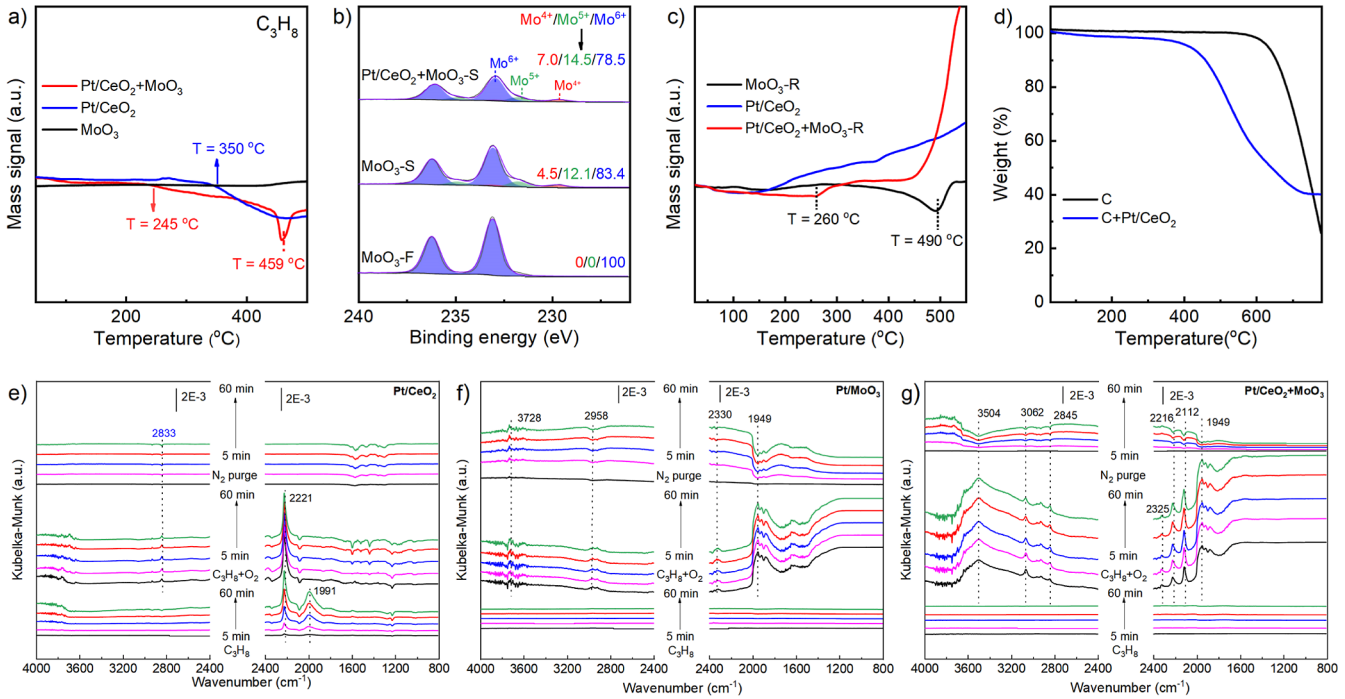

Figure 3. (a) Oxygen-free C_3H_8-TPSR profiles of Pt/CeO_2, MoO_3, and $Pt/CeO_2 + MoO_3$. (b) XPS spectra of Mo 3*d* of spent MoO_3, spent $Pt/CeO_2 + MoO_3$, and fresh MoO_3 (F = fresh and S = spent). (c) O_2-TPO profiles of MoO_3-R, Pt/CeO_2, and $Pt/CeO_2 + MoO_3$-R. (d) Activated carbon (or physically mixed catalyst) combustion test. (e−g) *In situ* DRIFTS of propane oxidation over Pt/CeO_2, Pt/MoO_3, and $Pt/CeO_2 + MoO_3$ catalysts at 250 °C.

MoO_3 changes the propane oxidation reaction pathway, even though the Pt and MoO_3 sites are spatially separated.

Given that MoO_3 significantly promotes Pt/CeO_2 for propane oxidation, it is necessary to know whether the mass ratio of Pt/CeO_2 to MoO_3 or the Pt content influences the catalytic reaction. Further optimization of the catalysis suggests that the suitable mass ratio of Pt/CeO_2 to MoO_3 is found to be 1:1 from Figure 1d. The Pt content in Pt/CeO_2 also affects the catalytic activity, more Pt sites benefit the propane oxidation reaction when Pt loading increases from 0.01 to 1 wt % (Figure 1e). Besides, long-term tests of Pt/MoO_3 and Pt/CeO_2 (280 °C for Pt/MoO_3 and 300 °C for Pt/CeO_2) are shown in Figure 1f. Both Pt/MoO_3 and Pt/CeO_2 exhibit robust stability in the propane oxidation reaction, suggesting that the active sites in these catalysts maintain their structural integrity even under humid conditions. Remarkably, Pt/MoO_3 maintains high activity for propane oxidation even under exposure to 100 ppm of SO_2, demonstrating its promising potential for practical applications (Figure S3).

3.2. Reaction Mechanism. Kinetic experiments were carried out on these catalysts to study the propane oxidation (Figure 2). The derived power law rate expressions are $r = 2.3 \times 10^{-7}\ [C_3H_8]^{1.0}[O_2]^{0.21}$ for Pt/MoO_3, $r = 0.7 \times 10^{-7}\ [C_3H_8]^{1.0}[O_2]^{-0.10}$ for Pt/CeO_2, and $r = 0.9 \times 10^{-7}\ [C_3H_8]^{1.0}[O_2]^{0.56}$ for $Pt/CeO_2 + MoO_3$ (Figure 2a,b, Table 1). The highest apparent rate constant (k) of Pt/MoO_3 is consistent with its highest specific mass reaction rate and lowest apparent activation energy (E_a) as shown in Figure 2. While the reaction orders for propane are consistently close to unity across these catalysts, owing to its weak adsorption on the catalyst surface, the reaction orders for oxygen exhibit significant variation. Most previous works observed that oxygen usually presents zero or negative reaction order as shown on Pt/CeO_2, indicating oxygen-saturated adsorption or preponderantly competitive adsorption.[35,47] This is ascribed to its stronger adsorption ability compared to propane on Pt active sites. However, the physically mixed $Pt/CeO_2 + MoO_3$ shows a different oxygen reaction order in comparison with the individual Pt/CeO_2, suggesting that the added MoO_3 component has entirely changed the reaction pathway for propane oxidation. It is generally accepted that Pt/CeO_2 itself is one of the most efficient catalysts for activating, storing, and releasing oxygen species, but Pt/CeO_2 is unfavorable for propane oxidation compared to Pt/MoO_3. Thus, it is inferred that MoO_3 can benefit the propane adsorption/activation as described in Figure 2d, while oxygen species are activated on Pt sites. As a result, competitive adsorption between O_2 and propane on Pt sites can be effectively avoided.

To further investigate the transfer of active oxygen species between spatially separated Pt and MoO_3 sites, we evaluated

https://doi.org/10.1021/acscatal.5c02534
ACS Catal. 2025, 15, 10746−10757

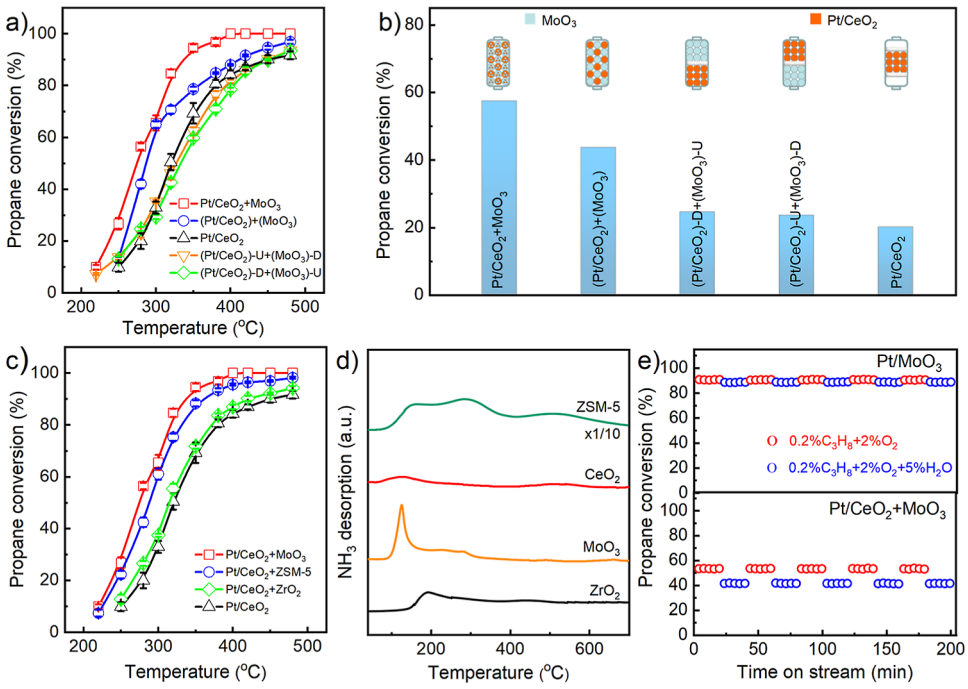

Figure 4. (a) Light-off curves of propane combustion over Pt/CeO_2, $Pt/CeO_2 + MoO_3$, $(Pt/CeO_2) + (MoO_3)$, (Pt/CeO_2)−U + (MoO_3)-D, and (Pt/CeO_2)-D +(MoO_3)−U. (b) Conversion of propane at 280 °C for different combinations of Pt/CeO_2 and MoO_3. (c) Light-off curves of propane oxidation over $Pt/CeO_2 + MoO_3$, Pt/CeO_2 + ZSM-5, $Pt/CeO_2 + ZrO_2$, and Pt/CeO_2. (d) NH_3-TPD profiles of MoO_3, ZSM-5, ZrO_2, and CeO_2. (e) Water tolerance test of Pt/MoO_3 and $Pt/CeO_2 + MoO_3$ at 280 °C.

the CO oxidation performance of Pt/CeO_2, Pt/MoO_3, and $Pt/CeO_2 + MoO_3$ (Figure S6). Notably, the addition of MoO_3 significantly suppresses the CO oxidation activity of Pt/CeO_2. This suppression mechanism originates from distinct reaction pathways. For Pt/CeO_2 systems, the adsorption and further reaction of CO/O_2 predominantly occur on Pt sites. The presence of MoO_3 nearby might create competitive oxygen migration channels, thus inducing the migration of active oxygen species from Pt sites to MoO_3 domains. Less reactive oxygen species available for CO result in a decrease in the CO oxidation activity. These findings also support our conclusion that active oxygen species can readily migrate between spatially separated Pt and MoO_3 sites.

To further confirm the propane oxidation mechanism on Pt sites and MoO_3, oxygen-free C_3H_8-TPSR profiles (Figure 3a) were recorded (at m/z = 29) for Pt/CeO_2, MoO_3, and $Pt/CeO_2 + MoO_3$. The individual MoO_3 is inactive for propane oxidation, and Pt/CeO_2 catalyzes propane oxidation starting at a temperature of 350 °C, which is ascribed to active Pt particles in Pt/CeO_2. Obviously, the temperature of propane oxidation decreases to 245 °C when MoO_3 is physically mixed with Pt/CeO_2. One explanation is that oxygen species activated on Pt/CeO_2 transfers to the MoO_3 surface and promotes the oxidation of propane. Mo 3*d* XPS spectra of catalysts were analyzed (Figures 3b and S4) after the C_3H_8-TPSR. It is found that only Mo^{6+} species exist in the fresh MoO_3 (denoted as MoO_3−F in Figure 3b), the components with binding energies at 233.0 and 236.2 eV are ascribed to Mo $3d_{5/2}$ and Mo $3d_{3/2}$ of Mo^{6+} species.[48] After the C_3H_8-TPSR test, XPS analysis reveals the presence of reduced Mo species, including Mo^{5+} (with Mo $3d_{5/2}$ at 231.7 eV and Mo $3d_{3/2}$ at 234.9 eV) and Mo^{4+} (with Mo $3d_{5/2}$ at 229.7 eV and Mo $3d_{3/2}$ at 232.9 eV),[49,50] particularly for the spent Pt/CeO_2+MoO_3 (denoted as $Pt/CeO_2 + MoO_3$−S in Figure 3b), indicating that the redox reaction of hydrocarbons occurs on the MoO_3 surface.

Oxygen-involving C_3H_8-TPSR profiles were also recorded as shown in Figure S7. The individual MoO_3 still remains inactive for propane oxidation, but the physically mixed MoO_3 decreases the starting oxidation temperature of propane from 230 to 220 °C of Pt/CeO_2, and the temperature window ΔT (from starting oxidation to complete oxidation) is also narrowed. Compared to individual Pt/CeO_2, the signal of methane intermediate appears at a lower temperature for Pt/CeO_2+MoO_3, further confirming MoO_3 promotes propane activation. In contrast, methane formation is undetectable for the individual MoO_3, as continuous propane activation and cracking on MoO_3 require active oxygen species derived from Pt sites.

The XPS spectra of Pt 4*f* reveal that the spent individual Pt/CeO_2 (denoted as Pt/CeO_2−S) and Pt/MoO_3 (denoted as Pt/MoO_3−S) catalysts exhibit a higher proportion of Pt^0 species compared to their fresh counterparts (Figure S8). This observation can be attributed to the reduction of oxidized Pt species by propane or its hydrocarbon intermediates during the reaction process. Such findings are consistent with numerous reports in the literature,[8,18] where similar reduction phenomena of Pt sites have been well-documented for Pt-based catalytic propane oxidation. Pt/MoO_3−S exhibits a higher proportion of Pt^0 species compared to Pt/CeO_2−S, consistent with its superior propane oxidation activity. Interestingly, the spent Pt/CeO_2+MoO_3 (denoted as Pt/CeO_2+MoO_3−S) demonstrates significantly a decreased Pt^0 proportion compared to the fresh Pt/CeO_2, which is very distinct from the individual Pt/CeO_2−S. This observation suggests that in $Pt/CeO_2 + MoO_3$, propane activation and oxidation predominantly occur on the MoO_3 surface while O_2 is activated on Pt sites, resulting in more oxidation state Pt

https://doi.org/10.1021/acscatal.5c02534
ACS Catal. 2025, 15, 10746−10757

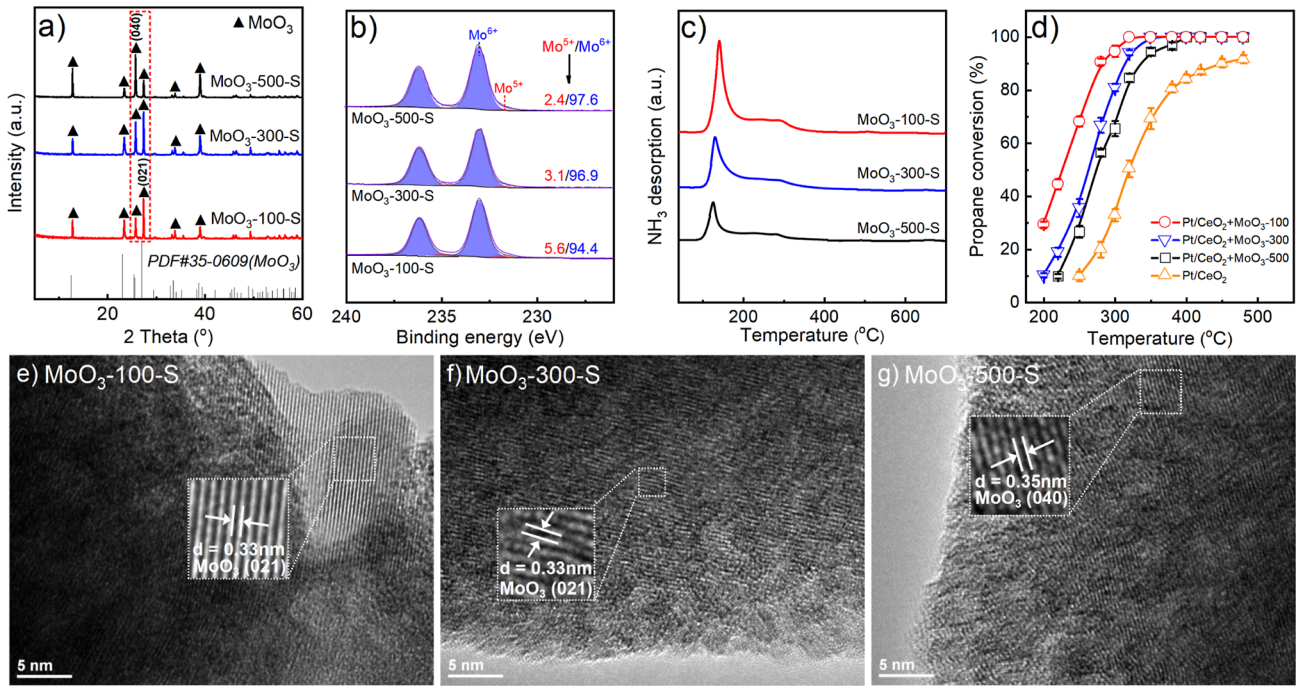

Figure 5. (a) XRD patterns. (b) XPS spectra of Mo 3*d*. (c) NH_3-TPD profiles of MoO_3-100-S, MoO_3-300-S, and MoO_3-500-S (S = spent). (d) Light-off curves of propane oxidation over Pt/CeO_2 physically mixed with different MoO_3. HRTEM images of (e) MoO_3-100-S, (f) MoO_3-300-S, and (g) MoO_3-500-S.

formed. In contrast, the Pt sites in the individual Pt/CeO_2 species play a dominant role in propane activation and oxidation, leading to a more pronounced reduction of Pt species.

To identify oxygen species being transferred from Pt/CeO_2 to MoO_3 through their contact interface, MoO_3 was first reduced by H_2 (denoted as MoO_3-R) and then conducted on O_2-TPO (Figure 3c). The individual Pt/CeO_2 shows a negative peak at low temperatures corresponding to the gaseous oxygen being stored in the catalyst, but the stored oxygen species in Pt/CeO_2 is gradually released when the temperature is beyond 200 °C. For the individual MoO_3-R, a few surface Mo atoms of MoO_3-R are oxidized at nearly 180 °C, and the bulk atoms of MoO_3-R are oxidized at a high temperature of 490 °C. It is obviously found that the oxidation temperature of bulk MoO_3-R decreases to 260 °C when physically mixed with Pt/CeO_2. Compared to the individual Pt/CeO_2, much more oxygen species are released from Pt/CeO_2+MoO_3-R when the temperature is beyond 450 °C. The above results suggest that active oxygen species transferred from Pt/CeO_2 promote the oxidation of MoO_3-R and that more active oxygen species are stored in the Pt/CeO_2 + MoO_3-R system. Additionally, Pt/CeO_2 was physically mixed with activated carbon (C), and it is also confirmed that the active oxygen species could be transferred through their contact interface and promote the combustion of activated carbon (Figure 3d).

The *in situ* DRIFT spectra of propane oxidation were carried out under staged atmosphere conditions (C_3H_8, C_3H_8 + O_2, and N_2) over Pt/CeO_2, Pt/MoO_3, and Pt/CeO_2 + MoO_3 at 250 °C to further study the reaction pathway (Figure 3e–g), and the stacked spectra mean signal recorded at different times in each step. The vibration peak at 1991 cm^{-1} during the oxygen-free propane purge corresponds to the linear adsorption of intermediate CO on the metal Pt atoms for Pt/CeO_2, and the vibration peak of gaseous CO_2 at 2221 cm^{-1} suggests that the active oxygen stored in Pt/CeO_2 enables the complete oxidation of propane. The vibration intensity of CO_2 increases when gaseous oxygen is introduced into feed gas due to more CO_2 generation.[51,52] The bands within the range of 1700−1900 cm^{-1} are ascribed to the carbonates generated on the MoO_3 surface for Pt/MoO_3.[29] Pt/CeO_2 + MoO_3 also shows such bands during propane oxidation, suggesting that the MoO_3 surface provides active sites for propane oxidation and carbonate generation. This evidence also confirms that propane is activated on the MoO_3 surface.

3.3. Effect of Pt Sites and MoO_3 Distance. To study the effect of Pt sites and MoO_3 distance on the catalytic activity, Pt/CeO_2 and MoO_3 are mixed in different combination ways to catalyze propane oxidation (Figure 4a,b). The schematic diagrams of different catalyst combinations for propane oxidation are listed in Table S2. Namely, the powders of Pt/CeO_2 and MoO_3 were directly physically mixed and then pressed and sieved to 60−80 mesh, denoted as Pt/CeO_2+MoO_3. The powders of Pt/CeO_2 and MoO_3 were separately pressed and sieved to 60−80 mesh, then physically mixed, denoted as (Pt/CeO_2) + (MoO_3). The individual sieved Pt/CeO_2 and MoO_3 particles were loaded in a fix bed upper and down layer, respectively, denoted as (Pt/CeO_2)−U + (MoO_3)-D. On the contrary, it is denoted as (Pt/CeO_2)-D + (MoO_3)−U. Propane oxidation activities on these catalysts are in the order of Pt/CeO_2 + MoO_3 > (Pt/CeO_2) + (MoO_3) > Pt/CeO_2 ≈ (Pt/CeO_2)−U + (MoO_3)-D ≈ (Pt/CeO_2)-D + (MoO_3)−U; this result suggests that the distance of Pt sites and MoO_3 significantly affects the catalytic performance for propane oxidation. The synergistic catalysis between Pt sites and MoO_3 is more significant when they are in close contact. To further confirm the influence of the surface property of the combined oxides, Pt/CeO_2 is also physically combined with other components (ZSM-5, ZrO_2) for propane oxidation. It is

https://doi.org/10.1021/acscatal.5c02534
ACS Catal. 2025, 15, 10746−10757

found that the ZrO_2 surface with few acid sites cannot enhance the activity of Pt/CeO_2, whereas the well-known acid material of ZSM-5 physically mixed Pt/CeO_2 remarkably increases the catalytic activity.[17,53,54] Such results suggest that the acid sites in MoO_3 play a crucial role in propane activation. Notably, acid material ZSM-5 possesses more acid sites than MoO_3 according to the results of NH_3-TPD; MoO_3 with better oxygen mobility than ZSM-5 accounts for the superior activity of Pt/CeO_2 + MoO_3 than Pt/CeO_2 + ZSM-5 (Figure 4d). Moreover, the water tolerance of the catalyst is also affected by the distance of Pt and MoO_3 sites. The Pt/MoO_3 with a shorter distance of Pt and MoO_3 sites shows better performance (Figure 4e).

3.4. Effect of MoO_3 Defect Concentration. From Figure 3b, Mo species with lower oxidation states would be generated during propane; thus, the defect concentration of MoO_3 may also affect the catalytic reaction. To further study the effect of MoO_3 surface defects, the preparation method of MoO_3 was modified to change the surface property of MoO_3.[29,55] The precursor of Mo ($(NH_4)_6Mo_7O_{24}{\cdot}4H_2O$) was first pretreated at 100 °C to obtain $(NH_4)_8Mo_{10}O_{34}$; then, the pressed and sieved $(NH_4)_8Mo_{10}O_{34}$ (60−80 mesh) was physically mixed with Pt/CeO_2. The *in situ* generated MoO_3 during the propane oxidation reaction was denoted as MoO_3-100-S. Similarly, the *in situ* generated MoO_3 derived from $(NH_4)_6Mo_7O_{24}{\cdot}4H_2O$ pretreated at 300 and 500 °C is denoted as MoO_3-300-S and MoO_3-500-S, respectively. From the XRD patterns of different MoO_3 samples, the characteristic diffraction peaks at 12.7, 23.3, 23.7, and 27.3° are ascribed to the orthorhombic phase of α-MoO_3 (PDF no. 35-0609), and the diffraction peaks at 25.7 and 27.3° are ascribed to the (040) and (021) facets of MoO_3, respectively (Figure 5a). It is clearly observed that the intensity of the diffraction peak corresponding to the MoO_3 (040) facet increases but that of the MoO_3 (021) facet decreases when the pretreatment temperature of MoO_3 increases from 100 to 500 °C. In addition, MoO_3 (040) is more visible in MoO_3-500-S, but MoO_3 (021) dominates in MoO_3-100-S from the HRTEM images (Figure 5e−g). According to the XPS result of Mo 3*d* spectra (Figure 5b), it is found that more Mo^{5+} species, associating with more defects, are generated when more MoO_3 (021) facets are exposed. EPR experiments were also carried out to study the defect concentration, as shown in Figure S9. The signal of oxygen vacancy is clearly observed at g = 2.002,[56,57] the increasing signal means increment of surface oxygen vacancy concentration in the catalyst; thus, the surface oxygen vacancy concentration of these catalysts is in order of MoO_3-100-S > MoO_3-300-S > MoO_3-500-S, which is consistent with the XPS results. The NH_3-TPD result suggests that a preferentially exposed MoO_3 (021) facet leads to enhanced surface acidity of MoO_3 (Figure 5c). The activities of Pt/CeO_2 combined with different MoO_3 samples show that the MoO_3 (021) facet can better facilitate the oxidation of propane, which should be related to the generation of more acid sites derived by surface defects (Figure 5d). The *in* situ DRIFTS spectra of propane oxidation were conducted over Pt/CeO_2 + MoO_3 with varying MoO_3 defect concentrations (MoO_3-500-S and MoO_3-100-S) at different reaction temperatures (Figure S10). The characteristic peak at 2964 cm^{-1}, attributed to the C−H bond vibration of gaseous propane, disappears at a lower temperature for Pt/CeO_2 + MoO_3-100-S compared to that for Pt/CeO_2 + MoO_3-500-S, indicating faster propane consumption on the former. Furthermore, the carbonate-related signals are significantly weaker for Pt/CeO_2 + MoO_3-100-S, suggesting the rapid decomposition of reaction intermediates during propane oxidation. These results demonstrate that the structural features of the MoO_3 (021) surface play a critical role in enhancing the catalytic activity for propane oxidation.

3.5. Density Functional Theory Calculation. To gain a profound understanding of the critical role of α-MoO_3 in propane adsorption and activation, we employed DFT calculations to systematically investigate the adsorption of O_2 and propane on different surfaces (Pt_{13}/CeO_2, MoO_3 (021), and MoO_3 (010)). Based on the well-established Langmuir−Hinshelwood (L-H) mechanism for propane oxidation, we constructed an O_2 and propane dual molecule adsorption model on catalysts considering two key factors: (1) the preferential exposure of MoO_3 (040) facets in MoO_3-500-S and MoO_3 (021) facets in MoO_3-100-S based on the XRD result, (2) the predominant presence of the Pt_{13} cluster in the Pt/CeO_2 catalyst. Thus, we focus on the adsorption of O_2 and propane on the Pt_{13} cluster and these MoO_3 surfaces. Figure 6a,b displays the structures of the MoO_3 (010) and MoO_3 (021) surface. In our DFT calculations, we used the MoO_3 (010) surface as the model instead of the MoO_3 (040) surface because the catalytic reaction occurs on the catalyst surface, and the exposed active sites on MoO_3 (010) are identical to those on MoO_3 (040). For MoO_3 (010), we constructed the terminal oxygen defects, which are consistent with the results reported in the literature.[58] It is found that the MoO_3 (010) surface primarily consists of six-coordinated Mo species (marked as Mo−O_6), corresponding to the high oxidation state Mo^{6+}, while also containing a small amount of five-coordinated Mo (marked as Mo−O_5) species. For MoO_3 (021), the surface exhibits a higher proportion of Mo−O_5 and four-coordinated Mo species (marked as Mo−O_4), which are associated with the lower oxidation state Mo. This observation aligns with the XPS results discussed in Figure 5b.

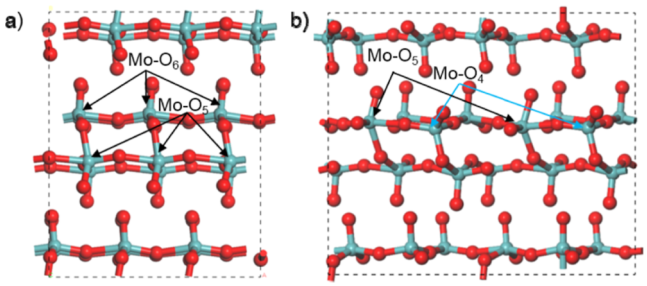

Figure 6. Structures of (a) MoO_3 (010) and (b) MoO_3 (021) surfaces (Mo−O_6: six-coordinated Mo, Mo−O_5: five-coordinated Mo, and Mo−O_4: four-coordinated Mo).

Figure 7a,b shows the adsorption of O_2 on different active sites (Pt_{13} clusters and MoO_3 surfaces). Our calculations reveal that the adsorption energies of O_2 and propane on Pt clusters are −1.111 and −0.368 eV, respectively. The significantly lower adsorption energy of O_2 suggests that O_2 can competitively absorb propane on Pt clusters, which aligns with our kinetic results for propane oxidation. The O−O bond length elongates from 1.22 Å in the gas phase to 1.38 Å upon adsorption on Pt clusters, indicating strong adsorption and activation of O_2 on Pt sites. Besides, the adsorption energies of O_2 on MoO_3 (010) and MoO_3 (021) are only −0.074 and −0.151 eV, respectively, suggesting a strong preferential adsorption of O_2 at Pt sites compared to MoO_3 surfaces.

https://doi.org/10.1021/acscatal.5c02534
ACS Catal. 2025, 15, 10746−10757

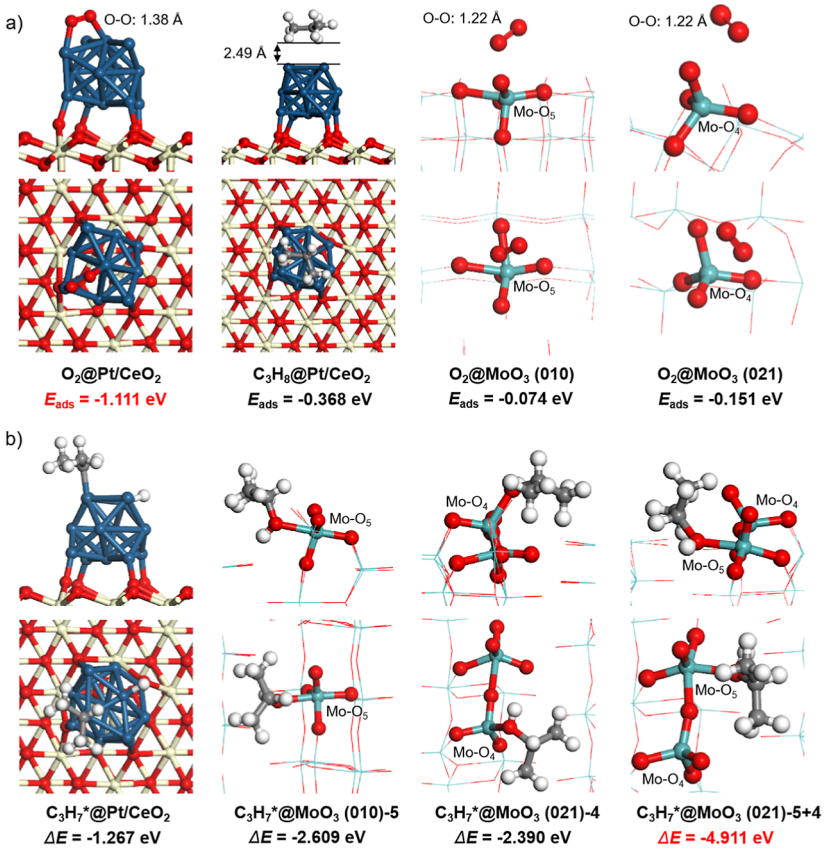

Figure 7. (a) O_2 and propane adsorbed on Pt/CeO_2 and MoO_3 surfaces. (b) Propane dissociation over Pt/CeO_2 and MoO_3 surfaces. (E_{ads} and ΔE represent the adsorption energy and reaction energy, respectively.).

The rate-determining step for propane oxidation is well established to be the cleavage of the first C−H bond in propane. The reaction energy (ΔE) of first C−H bond cleavage in propane was calculated to study the reaction possibility of propane activated on these active sites.[59] The reaction energy (ΔE) for propane activation at Pt sites is calculated to be −1.267 eV, demonstrating their exceptional catalytic potential for C−H bond activation in the absence of competitive adsorption. The reaction energy (ΔE) becomes more negative at −2.609 and −2.390 eV when propane interacts with Mo−O_5 sites on MoO_3 (010) and Mo−O_4 sites on MoO_3 (021), respectively. More remarkably, the first C−H bond cleavage of propane exhibits the most negative reaction energy (−4.911 eV) when facilitated by synergistic cooperation between five- and four-coordinated Mo sites on the MoO_3 (021) surface. This pronounced thermodynamic favorability explains the superior catalytic activity of Pt_{13}/CeO_2 + MoO_3-100-S in propane oxidation. Therefore, our calculations further demonstrate that Pt sites present stronger adsorption and activation ability for O_2, whereas MoO_3 has a higher ability for propane activation. This dual functionality significantly enhances the overall propane oxidation efficiency by simultaneously addressing two critical factors: (1) eliminating competitive adsorption between O_2 and propane through site segregation and (2) strengthening propane activation on the optimal MoO_3 surface.

Therefore, the detailed reaction mechanism for propane oxidation over the combined Pt/CeO_2 and MoO_3 catalyst is illustrated in Scheme 1. The process is initiated with the preferential adsorption of O_2 on Pt sites and propane on the

Scheme 1. Proposed Reaction Mechanism of Propane Oxidation over the Combined Pt/CeO_2 and MoO_3 Catalysts

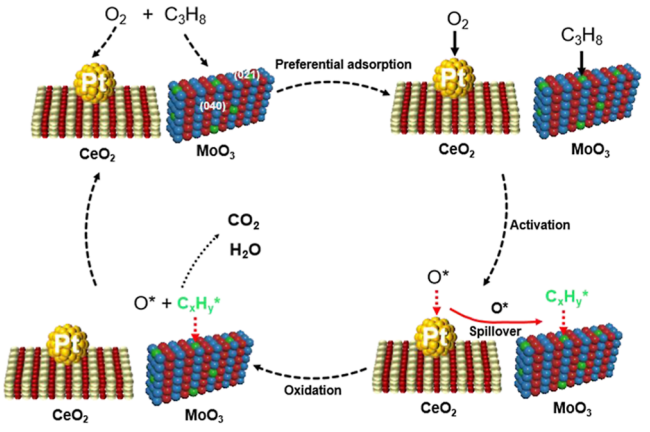

MoO_3 (021) surface. Subsequently, propane undergoes dissociation, generating activated hydrocarbon species that remain bound to the five and four coordinated Mo sites on the MoO_3 (021) surface. Concurrently, activated oxygen species migrate from the Pt sites to the MoO_3 surface. Finally, the activated hydrocarbon species react with the transferred oxygen species to form CO_2 and H_2O, while the Mo sites are regenerated for subsequent catalytic cycles.

4. CONCLUSION

In summary, the mechanistic details of synergistic catalysis on MoO_3 as acid sites and Pt nanoparticles as oxygen activation

https://doi.org/10.1021/acscatal.5c02534
ACS Catal. 2025, 15, 10746−10757

sites have been systematically investigated in propane combustion. Specifically, surface acid sites on defective MoO_3 supports play very vital roles in propane adsorption/activation. Pt sites activate the gaseous oxygen; oxygen spillover from Pt sites to the MoO_3 surface significantly promotes the catalytic combustion of the activated hydrocarbons. This reaction pathway can effectively alleviate the competitive adsorption between oxygen and propane on Pt sites, thus significantly boosting propane combustion activity. Moreover, it is found that the distance between Pt and MoO_3 sites and the density of surface acid sites on MoO_3 can remarkably affect the catalytic performance of catalysts. The surface acid site density of MoO_3 is dependent on the surface defect concentration of MoO_3. This work provides deep insight into the individual functionality and synergistic effects of redox site−acid site in the catalytic combustion of light alkane.

■ ASSOCIATED CONTENT

Supporting Information

The Supporting Information is available free of charge at https://pubs.acs.org/doi/10.1021/acscatal.5c02534.

XRD patterns, Raman spectra, HRTEM images, physical−chemical parameters of catalysts, SO_2 tolerance test, XPS spectra of Mo 3*d* and Pt 4*f*, CO oxidation test, C_3H_8-TPSR profiles, EPR profiles, *in situ* DRIFTS of propane oxidation, schematic diagram of catalyst combination, and kinetic data (PDF)

■ AUTHOR INFORMATION

Corresponding Authors

Mao-Di Wang − *Key Laboratory of the Ministry of Education for Advanced Catalysis Materials, Zhejiang Key Laboratory of Advanced Catalysis and Adsorption Materials, Zhejiang Normal University, Jinhua 321004, China*; Email: maodiwang@zjnu.edu.cn

Wei Tan − *State Key Laboratory of Water Pollution Control and Green Resource Recycling, School of Environment, Jiangsu Key Laboratory of Vehicle Emissions Control, Centre for Shared Scientific Research Facilities, Key Laboratory of Mesoscopic Chemistry of MOE, School of Chemistry and Chemical Engineering, Nanjing University, Nanjing 210023, China*; orcid.org/0000-0002-1481-9346; Email: tanwei@nju.edu.cn

Jian Chen − *Key Laboratory of the Ministry of Education for Advanced Catalysis Materials, Zhejiang Key Laboratory of Advanced Catalysis and Adsorption Materials, Zhejiang Normal University, Jinhua 321004, China*; orcid.org/0000-0001-5982-044X; Email: jianchen@zjnu.cn

Authors

Cai-Hao Wen − *Key Laboratory of the Ministry of Education for Advanced Catalysis Materials, Zhejiang Key Laboratory of Advanced Catalysis and Adsorption Materials, Zhejiang Normal University, Jinhua 321004, China*

Lin-Ya Xu − *Key Laboratory of the Ministry of Education for Advanced Catalysis Materials, Zhejiang Key Laboratory of Advanced Catalysis and Adsorption Materials, Zhejiang Normal University, Jinhua 321004, China*

Yao-Dong Hao − *Key Laboratory of the Ministry of Education for Advanced Catalysis Materials, Zhejiang Key Laboratory of Advanced Catalysis and Adsorption Materials, Zhejiang Normal University, Jinhua 321004, China*

Qian Zhou − *Key Laboratory of the Ministry of Education for Advanced Catalysis Materials, Zhejiang Key Laboratory of Advanced Catalysis and Adsorption Materials, Zhejiang Normal University, Jinhua 321004, China*

Yi-Wei Xian − *Key Laboratory of the Ministry of Education for Advanced Catalysis Materials, Zhejiang Key Laboratory of Advanced Catalysis and Adsorption Materials, Zhejiang Normal University, Jinhua 321004, China*

Lin Dong − *State Key Laboratory of Water Pollution Control and Green Resource Recycling, School of Environment, Jiangsu Key Laboratory of Vehicle Emissions Control, Centre for Shared Scientific Research Facilities, Key Laboratory of Mesoscopic Chemistry of MOE, School of Chemistry and Chemical Engineering, Nanjing University, Nanjing 210023, China*; orcid.org/0000-0002-8393-6669

Meng-Fei Luo − *Key Laboratory of the Ministry of Education for Advanced Catalysis Materials, Zhejiang Key Laboratory of Advanced Catalysis and Adsorption Materials, Zhejiang Normal University, Jinhua 321004, China*; orcid.org/0000-0002-9331-701X

Qi-Hua Yang − *Key Laboratory of the Ministry of Education for Advanced Catalysis Materials, Zhejiang Key Laboratory of Advanced Catalysis and Adsorption Materials, Zhejiang Normal University, Jinhua 321004, China*; orcid.org/0000-0002-1118-3397

Complete contact information is available at: https://pubs.acs.org/10.1021/acscatal.5c02534

Notes

The authors declare no competing financial interest.

■ ACKNOWLEDGMENTS

This work was financially supported by the National Natural Science Foundation of China (No. 22172145, 22306090), the Leading Innovative and Entrepreneur Team Introduction Program of Zhejiang (no. 2022R01007), and the Financial Support by Research Fund of Key Laboratory of the Ministry of Education for Advanced Catalysis Materials, Zhejiang Key Laboratory of Advanced Catalysis and Adsorption Materials, Zhejiang Normal University.

■ REFERENCES

(1) Wang, Z.; Huang, Z.; Brosnahan, J. T.; Zhang, S.; Guo, Y.; Guo, Y.; Wang, L.; Wang, Y.; Zhan, W. Ru/CeO_2 catalyst with optimized CeO_2 support morphology and surface facets for propane combustion. *Environ. Sci. Technol.* **2019**, *53*, 5349−5358.

(2) Liu, S.; Wang, H.; Wang, S.; Dai, Y.; Liu, B.; Liu, Y.; Dang, F.; Smith, K. J.; Nie, X.; Hou, S.; Guo, X. Engineering morphology and Ni substitution of $Ni_xCo_{3-x}O_4$ spinel oxides to promote catalytic combustion of ethane: Elucidating the influence of oxygen defects. *ACS Catal.* **2023**, *13*, 4683−4699.

(3) Gu, H.; Lan, J.; Hu, H.; Jia, F.; Ai, Z.; Zhang, L.; Liu, X. Surface oxygen vacancy-dependent molecular oxygen activation for propane combustion over α-MnO_2. *J. Hazard. Mater.* **2023**, *460*, 132499.

(4) Choudhary, V. R.; Deshmukh, G. M.; Pataskar, S. G. Low-temperature complete combustion of a dilute mixture of methane and propane over transition-metal-doped ZrO_2 catalysts: Effect of the presence of propane on methane combustion. *Environ. Sci. Technol.* **2005**, *39*, 2364−2368.

(5) Zhu, Z.; Lu, G.; Guo, Y.; Guo, Y.; Zhang, Z.; Wang, Y.; Gong, X. High performance and stability of the Pt-W/ZSM-5 catalyst for the

total oxidation of propane: The role of tungsten. *ChemCatChem* **2013**, *5*, 2495−2503.
(6) Chen, W.; Zheng, J.; Fang, Y.; Wang, Y.; Hu, J.; Zhu, Y.; Zhu, X.; Li, W.; Zhang, Q.; Pan, C.; Zhang, B.; Qiu, X.; Wang, S.; Cui, S.; Wang, J.; Wu, J.; Luo, Z.; Guo, Y. Role of the in-situ-formed surface (Pt-S-O)-Ti active structure in SO_2-Promoted C_3H_8 combustion over a Pt/TiO_2 catalyst. *Environ. Sci. Technol.* **2024**, *58*, 3041−3053.
(7) Hao, H.; Jin, B.; Liu, W.; Wu, X.; Yin, F.; Liu, S. Robust Pt@TiO_x/TiO_2 catalysts for hydrocarbon combustion: Effects of Pt-TiO_x interaction and sulfates. *ACS Catal.* **2020**, *10*, 13543−13548.
(8) Liu, Y.; Li, X.; Liao, W.; Jia, A.; Wang, Y.; Luo, M.; Lu, J. Highly active Pt/BN catalysts for propane combustion: The roles of support and reactant-induced evolution of active sites. *ACS Catal.* **2019**, *9*, 1472−1481.
(9) Yang, A.; Zhu, H.; Li, Y.; Cargnello, M. Support acidity improves Pt activity in propane combustion in the presence of steam by reducing water coverage on the active sites. *ACS Catal.* **2021**, *11*, 6672−6683.
(10) Ge, S.; Fan, W.; Tang, X.; Cui, Y.; Wang, D.; Gong, X.; Dai, S.; Lou, Y.; Tang, J.; Guo, Y.; Zhan, W.; Wang, L.; Guo, Y. Revealing the size effect of ceria nanocube-supported platinum nanoparticles in complete propane oxidation. *ACS Catal.* **2024**, *14*, 2532−2544.
(11) Yang, A.; Streibel, V.; Choksi, T. S.; Aljama, H.; Werghi, B.; Bare, S. R.; Sánchez-Carrera, R. S.; Schäfer, A.; Li, Y.; Abild-Pedersen, F.; Cargnello, M. Insights and comparison of structure−property relationships in propane and propene catalytic combustion on Pd- and Pt-based catalysts. *J. Catal.* **2021**, *401*, 89−101.
(12) Wang, A.; Ding, J.; Li, M.; Song, P.; Zhao, Z.; Guo, Y.; Guo, Y.; Wang, L.; Dai, Q.; Zhan, W. Robust Ru/Ce@Co catalyst with an optimized support structure for propane oxidation. *Environ. Sci. Technol.* **2024**, *58*, 12742−12753.
(13) Fu, Q.; Wang, S.; Wang, T.; Xing, D.; Yue, X.; Wang, M.; Wang, S. Insights into the promotion mechanism of ceria-zirconia solid solution to ethane combustion over Pt-based catalysts. *J. Catal.* **2022**, *405*, 129−139.
(14) Li, B.; Zhao, X.; Luo, X.; Zhang, W.; Wen, C.; Xu, L.; Tang, C.; Luo, M.; Chen, J. Boosting propane combustion over Pt/WO_3 catalyst by activating interface oxygen species. *Appl. Surf. Sci.* **2024**, *650*, 159225.
(15) Ge, S.; Fan, W.; Tang, X.; Cui, Y.; Wang, D.; Gong, X.; Dai, S.; Lou, Y.; Tang, J.; Guo, Y.; Zhan, W.; Wang, L.; Guo, Y. Revealing the size effect of ceria nanocube-supported platinum nanoparticles in complete propane oxidation. *ACS Catal.* **2024**, *14*, 2532−2544.
(16) Wen, C.; Xu, L.; Zhao, W.; Xu, H.; Zhao, X.; Zhou, Q.; Tang, C.; Jia, W.; Luo, M.; Chen, J. Novel strategy to regulate the geometric and electronic structure of Pt catalyst for efficient propane combustion. *Appl. Catal., A* **2024**, *680*, 119778.
(17) Wang, X.; Liu, C.; He, L.; Li, B.; Lu, J.; Luo, M.; Chen, J. Unveiling geometric and electronic effects of Pt species on water-tolerant Pt/ZSM-5 catalyst for propane oxidation. *Appl. Catal., A* **2023**, *655*, 119108.
(18) Li, X.; Liu, Y.; Liao, W.; Jia, A.; Wang, Y.; Lu, J.; Luo, M. Synergistic roles of Pt^0 and Pt^{2+} species in propane combustion over high-performance Pt/AlF_3 catalysts. *Appl. Surf. Sci.* **2019**, *475*, 524−531.
(19) Avila, M.; Vignatti, C.; Apesteguía, C.; Garetto, T. Effect of support on the deep oxidation of propane and propylene on Pt-based catalysts. *Chem. Eng. J.* **2014**, *241*, 52−59.
(20) Yoshida, H.; Yazawa, Y.; Takagi, N.; Satsuma, A.; Tanaka, T.; Yoshida, S.; Hattori, T. XANES study of the support effect on the state of platinum catalysts. *J. Synchrotron Radiat.* **1999**, *6*, 471−473.
(21) Dong, J.; Li, D.; Zhang, Y.; Chang, P.; Jin, Q. Insights into the CeO_2 facet-depended performance of propane oxidation over Pt-CeO_2 catalysts. *J. Catal.* **2022**, *407*, 174−185.
(22) Yazawa, Y.; Takagi, N.; Yoshida, H.; Komai, S.; Satsuma, A.; Tanaka, T.; Yoshida, S.; Hattori, T. The support effect on propane combustion over platinum catalyst: Control of the oxidation-resistance of platinum by the acid strength of support materials. *Appl. Catal., A* **2002**, *233*, 103−112.
(23) Yazawa, Y.; Yoshida, H.; Hattori, T. The support effect on platinum catalyst under oxidizing atmosphere: Improvement in the oxidation-resistance of platinum by the electrophilic property of support materials. *Appl. Catal., A* **2002**, *237*, 139−148.
(24) Wang, W.; Li, D.; Yu, H.; Liu, C.; Tang, C.; Chen, J.; Lu, J.; Luo, M. Insights into different reaction behaviors of propane and CO oxidation over Pt/CeO_2 and Pt/Nb_2O_5: The crucial roles of support properties. *J. Phys. Chem. C* **2021**, *125*, 19301−19310.
(25) Sun, J.; Mu, C.; Guo, D.; Zhao, Y.; Wang, S.; Ma, X. Effects of intimacy between acid and metal sites on the isomerization of n-C16 at the large/minor nanoscale and atomic scale. *ACS Catal.* **2022**, *12*, 4092−4102.
(26) Zhang, F.; Zeng, M.; Yappert, R.; Sun, J.; Lee, Y.; Lapointe, A.; Peters, B.; Abu-omar, M.; Scott, S. Polyethylene upcycling to long-chain alkylaromatics by tandem hydrogenolysis/aromatization. *Science* **2020**, *370*, 437−441.
(27) Tang, Z.; Zhang, T.; Luo, D.; Wang, Y.; Hu, Z.; Yang, R. Catalytic combustion of methane: From mechanism and materials properties to catalytic performance. *ACS Catal.* **2022**, *12*, 13457−13474.
(28) Peng, Q.; Han, W.; Han, W.; Dong, F.; Tang, Z.; Zhou, Z. Tailored Pt/NiaCobAlO_x catalysts derived from LDH structure for efficient catalytic combustion of propane. *Chem. Eng. J.* **2024**, *500*, 157181.
(29) Liu, L.; Han, W.; Dong, F.; Feng, H.; Tang, Z. Designing ordered mesoporous confined Pt/Ti0.1AlOy catalysts for the catalytic combustion of propane. *New J. Chem.* **2023**, *11*, 5519−5533.
(30) Zhao, P.; Chen, J.; Yu, H.; Cen, B.; Wang, W.; Luo, M.; Lu, J. Insights into propane combustion over MoO_3 promoted Pt/ZrO_2 catalysts: The generation of Pt-MoO_3 interface and its promotional role on catalytic activity. *J. Catal.* **2020**, *391*, 80−90.
(31) Liao, W.; Fang, X.; Cen, B.; Chen, J.; Liu, Y.; Luo, M.; Lu, J. Deep oxidation of propane over WO_3 promoted Pt/BN catalysts: The critical role of Pt-WO_3 interface. *Appl. Catal. B Environ. Energy* **2020**, *272*, 118858.
(32) Xu, L.; Zhou, Q.; Wen, C.; Xu, H.; Zhao, X.; Liu, F.; Luo, M.; Chen, J. Mechanistic understanding of oxygen spillover enables efficient propane combustion over Pt/$AlSO_x$ catalyst. *Sep. Purif. Technol.* **2025**, *354*, 129193.
(33) Xia, L.; Jian, Y.; Liu, Q.; Liu, Y.; Wang, J.; Chai, S.; Jing, M.; Albilali, R.; He, C. Boosted light alkane deep oxidation via metal bond length modulation-induced C−C bond preferential activation. *Environ. Sci. Technol.* **2024**, *58*, 3472−3482.
(34) Li, D.; Leng, X.; Wang, X.; Yu, H.; Zhang, W.; Chen, J.; Luo, M.; Lu, M. Unraveling the promoting roles of sulfate groups on propane combustion over Pt-SO_4^{2-}/ZrO_2 catalysts. *J. Catal.* **2022**, *407*, 322−332.
(35) Wang, X.; Xu, L.; Wen, C.; Li, D.; Li, B.; Lu, J.; Yang, Q.; Luo, M.; Chen, J. WO_3 boosted water tolerance of Pt nanoparticle on SO_4^{2-}-ZrO_2 for propane oxidation. *Appl. Catal. B Environ. Energy* **2023**, *338*, 123000.
(36) Xu, L.; Wen, C.; Luo, X.; Zhang, W.; Zhao, X.; Yang, Q.; Lu, J.; Luo, M.; Chen, J. Regulating the synergy of sulfate and Pt species in Pt/ZSM-5 for propane complete oxidation. *Appl. Catal. B Environ. Energy* **2024**, *354*, 124135.
(37) Burch, R.; Hayes, M. J. C-H bond activation in hydrocarbon oxidation on solid catalysts. *J. Mol. Catal. A: Chem.* **1995**, *100*, 13−33.
(38) Liu, X.; Zhang, M.; Liu, X.; Liu, J.; Dai, H.; Luo, W.; Liu, J.; Gao, R.; Yang, Q. Regulation of the properties of hydrogen dissociation and transfer in the presence of S atoms for efficient hydrogenations. *ACS Catal.* **2024**, *14*, 16214−16223.
(39) Kühne, T. D.; Iannuzzi, M.; Del Ben, M.; Rybkin, V. V.; Seewald, P.; Stein, F.; Laino, T.; Khaliullin, R. Z.; Schütt, O.; Schiffmann, F.; et al. CP2K: An electronic structure and molecular dynamics software package-Quickstep: Efficient and accurate electronic structure calculations. *J. Chem. Phys.* **2020**, *152*, 194103.
(40) Enkovaara, J.; Rostgaard, C.; Mortensen, J. J.; Chen, J.; Dułak, M.; Ferrighi, L.; Gavnholt, J.; Glinsvad, C.; Haikola, V.; Hansen, H. A.; et al. Electronic structure calculations with GPAW: a real-space

https://doi.org/10.1021/acscatal.5c02534
ACS Catal. 2025, 15, 10746−10757

implementation of the projector augmented-wave method. *J. Phys.: Condens. Matter* **2010**, *22*, 253202.
(41) Grimme, S.; Antony, J.; Ehrlich, S.; Krieg, H. A consistent and accurate ab initio parametrization of density functional dispersion correction (DFT-D) for the 94 elements H-Pu. *J. Chem. Phys.* **2010**, *132*, 154104.
(42) Ding, H.; Lin, H.; Sadigh, B.; Zhou, F.; Ozoliņš, V.; Asta, M. Computational investigation of electron small polarons in α-MoO_3. *J. Phys. Chem. C* **2014**, *118*, 15565−15572.
(43) Lu, J.; Jiang, X.; Hu, H.; Li, J. Norm-conserving 4f-in-core pseudopotentials and basis sets optimized for trivalent lanthanides (Ln = Ce-Lu). *J. Chem. Theory Comput.* **2023**, *19*, 82−96.
(44) Tan, W.; Xie, S.; Wang, X.; Xu, J.; Yan, Y.; Ma, K.; Cai, Y.; Ye, K.; Gao, F.; Dong, L.; Liu, F. Determination of intrinsic active sites on CuO-CeO_2-Al_2O_3 catalysts for CO oxidation and NO reduction by CO: Differences and connections. *ACS Catal.* **2022**, *12*, 12643−12657.
(45) Tan, W.; Xie, S.; Cai, Y.; Wang, M.; Yu, S.; Low, K.; Li, Y.; Ma, L.; Ehrlich, S. N.; Gao, F.; Dong, L.; Liu, F. Transformation of highly stable Pt single sites on defect engineered ceria into robust Pt clusters for vehicle emission control. *Environ. Sci. Technol.* **2021**, *55*, 12607−12618.
(46) Cai, Y.; Ji, X.; Zhang, B.; Mu, Y.; Tong, Q.; Liu, A.; Tan, W.; Liu, F.; Dong, L. Research progress in ceria-based catalysts for the selective catalytic oxidation of NH_3. *Sci. Sin. Chim.* **2024**, *54*, 295−308.
(47) Xian, Y.; Li, B.; Wen, C.; Xu, L.; Lu, W.; Zhou, Q.; Jia, W.; Luo, M.; Chen, J. Boosting propane combustion on dual active sites of Pt/WO3 through regulating Pt sites and activating propane on WO_3 surface. *Fuel* **2025**, *385*, 134172.
(48) Adamska, K.; Okal, J.; Tylus, W. Stable bimetallic Ru-Mo/Al_2O_3 catalysts for the light alkane combustion: Effect of the Mo addition. *Appl. Catal. B Environ. Energy* **2019**, *246*, 180−194.
(49) Cai, X.; Sang, X.; Song, Y.; Guo, D.; Liu, X.; Sun, X. Activating the highly reversible Mo^{4+}/Mo^{5+} redox couple in amorphous molybdenum oxide for high-performance supercapacitors. *ACS Appl. Mater. Interfaces* **2020**, *12*, 48565−48571.
(50) Xu, L.; Zhou, W.; Chao, S.; Liang, Y.; Zhao, X.; Liu, C.; Xu, J. Advanced oxygen-vacancy Ce-doped MoO_3 ultrathin nanoflakes anode materials used as asymmetric supercapacitors with ultrahigh energy density. *Adv. Energy Mater.* **2022**, *12*, 2200101.
(51) Pozdnyakova, O.; Teschner, D.; Wootsch, A.; Krohnert, J.; Steinhauer, B.; Sauer, H.; Toth, L.; Jentoft, F. C.; Knop-Gericke, A.; Paal, Z.; Schlögl, R. Preferential CO oxidation in hydrogen (PROX) on ceria-supported catalysts, part I: Oxidation state and surface species on Pt/CeO_2 under reaction conditions. *J. Catal.* **2006**, *237*, 1−16.
(52) Köck, E. M.; Kogler, M.; Bielz, T.; Klötzer, B.; Penner, S. *In situ* FT-IR spectroscopic study of CO_2 and CO adsorption on Y_2O_3, ZrO_2, and yttria-stabilized ZrO_2. *J. Phys. Chem. C* **2013**, *117*, 17666−17673.
(53) Han, W.; Lin, L.; Cen, Z.; Ke, Y.; Xu, Q.; Zhu, J.; Mei, X.; Xia, Z.; Zheng, X.; Wang, Y.; Liu, Y.; He, M.; Wu, H.; Han, B. Production of branched alkanes by upcycling of waste polyethylene over controlled acid sites of SO_4/ZrO_2-Al_2O_3 catalyst. *Angew. Chem., Int. Ed.* **2025**, *64*, No. e20241792.
(54) Zhao, M.; Wang, X.; Xu, J.; Li, Y.; Wang, X.; Chu, X.; Wang, K.; Wang, Z.; Zhang, L.; Feng, J.; Song, S.; Zhang, H. Strengthening the metal-acid interactions by using CeO_2 as regulators of precisely placing Pt species in ZSM-5 for furfural hydrogenation. *Adv. Mater.* **2024**, *36*, 2313596.
(55) Miao, Z.; Li, Z.; Zhao, J.; Si, W.; Zhou, J.; Zhuo, S. MoO_3 supported on ordered mesoporous zirconium oxophosphate: An efficient and reusability solid acid catalyst for alkylation and esterification. *Mol. Catal.* **2018**, *444*, 10−21.
(56) Nasser, R.; Zhou, H.; Li, F.; Elhouichet, H.; Song, J. Heterostructured MoO_3@$CoWO_4$ nanobelts towards high electromical performances via oxygen vacancies generation. *J. Colloid Interface Sci.* **2024**, *654*, 805−818.
(57) Shu, H.; Zhao, M.; Tang, C.; Ma, K.; Li, X. Atmosphere toward regulation of MoO_3 microstructure for lactic acid hydrodeoxygenation to propionic acid. *Inorg. Chem. Commun.* **2024**, *169*, 113015.
(58) Lei, Y.; Chen, Z. DFT + U study of properties of MoO_3 and hydrogen adsorption on MoO_3 (010). *J. Phys. Chem. C* **2012**, *116*, 25757−25764.
(59) Liu, J.; Su, H.; Sun, D.; Zhang, B.; Li, W. Crystallographic dependence of CO activation on cobalt catalysts: HCP versus FCC. *J. Am. Chem. Soc.* **2013**, *135*, 16284−16287.

https://doi.org/10.1021/acscatal.5c02534
ACS Catal. 2025, 15, 10746−10757